Available online at www.sciencedirect.com
ScienceDirect
Earth and Planetary Science Letters 250 (2006) 444–458
EPSL
www.elsevier.com/locate/epsl

Rock magnetic and geochemical proxies for iron mineral diagenesis in a tropical lake: Lago Verde, Los Tuxtlas, East–Central Mexico

Beatriz Ortega [a,*], Margarita Caballero [a], Socorro Lozano [b], Gloria Vilaclara [c], Alejandro Rodríguez [d]

[a] *Universidad Nacional Autonoma de Mexico, Instituto de Geofisica, 04510, Mexico DF, Mexico*
[b] *Universidad Nacional Autonoma de Mexico, Instituto de Geologia, 04510 Mexico, DF, Mexico*
[c] *Universidad Nacional Autonoma de Mexico, Facultad de Estudios Superiores de, Iztacala, Tlalnepantla, Edo, de Mexico, 54090, Mexico*
[d] *Universidad Nacional Autonoma de Mexico, Posgrado en Ciencias del Mar y, Limnologia, 04510 Mexico DF, Mexico*

Received 30 March 2006; received in revised form 22 August 2006; accepted 23 August 2006
Available online 27 September 2006
Editor: M.L. Delaney

Abstract

Magnetic and non-magnetic mineral analyses were conducted on a lacustrine sequence from Lago Verde in the tropical coast along the Gulf of Mexico that covers the last 2000 years. The site witnessed the transformation of the environment since the early Olmec societies until forest clearance in the last century. Through these analyses we investigated the processes that affected the magnetic mineralogy in order to construct a model of past environmental changes, and compare this model with the archeological record and inferred climatic changes in the northern hemisphere of tropical America. Volcanic activity has played a major influence on sediment magnetic properties, as a purveyor of Ti-magnetites/Ti-maghemites, and as a factor of instability in the environment. Anoxic reductive conditions are evident in most of Lago Verde's sedimentary record.

Direct observations of magnetic minerals and ratios of geochemical (Fe, Ti), and ferrimagnetic (χf) and paramagnetic (χp) susceptibility (χ) data, are used as parameters for magnetite dissolution ($\chi p/\chi$, Fe/χf), and precipitation (χf/Ti) of magnetic minerals. Intense volcanic activity and anoxia are recorded before A.D. 20, leading to the formation of framboidal pyrite. Increased erosion, higher evaporation rates, lower lake levels, anoxia and reductive diagenesis in non-sulphidic conditions are inferred for laminated sediments between A.D. 20–850. This deposit matches the period of historical crisis and multiyear droughts that contributed to the collapse of the Maya civilization. Dissolution of magnetite, a high organic content and framboidal pyrite point to anoxic, sulphidic conditions and higher lake levels after A.D. 850. Higher lake levels in Lago Verde broadly coincide with the increased precipitation documented during the Medieval Warm Period (A.D. 950–1350) in the northern tropical and subtropical regions of the American continent. For the Little Ice Age (A.D. 1400–1800), the relatively moist conditions inferred are in concordance with the glacial advances recorded in central Mexico. Higher erosion rates reflect destruction of the rainforest over the last 40 years.

Keywords: environmental magnetism; lake sediments; Los Tuxtlas; mineral diagenesis

* Corresponding author. Tel.: +52 55 56224232; fax: +52 55 555 09395.
E-mail address: bortega@geofisica.unam.mx (B. Ortega).

0012-821X/$ - see front matter © 2006 Elsevier B.V. All rights reserved.
doi:10.1016/j.epsl.2006.08.020

1. Introduction

The knowledge of past climatic and environmental conditions and their fluctuations is critical in order to understand the history of Mesoamerican cultures, as local environment characteristics partly affected the way in which these societies evolved. A history of environmental changes can also provide possible explanations for the causes that might have conditioned the settlement and abandonment of sites. For example, paleoclimatic records on lacustrine records [1–3] and laminated marine sediments [4], have linked dry multiyear periods to the Terminal Classic Maya demographic demise between A.D. 800 and 900 in the Yucatan peninsula.

Along central Mexico's gulf coast, the early Olmec civilization transformed to the posterior Epi-Olmec society between the Early Formative period (1500–900 B.C.) through the Late Classic period (A.D. 600–1000) [5]. Although extensive archeological research has been conducted for more than six decades in the Olmec area [e.g. 6,7], paleoenvironmental reconstructions are scarce [8,9]. However, several studies suggest that environmental causes such as volcanism [10], sea-level changes [11], earthquake-driven slumps [12] and hurricanes [13] have affected past and modern human settlements in this region.

Insights into paleoenvironmental conditions can be obtained from sediments by a range of combined magnetic and non-magnetic techniques, such as geochemical, pollen and diatom analysis [e.g. 14,15]. The magnetic methods investigate the mineralogy, concentration and grain size distribution of Fe-bearing minerals that contribute to the magnetic fraction in deposits from several environments.

However, as the interpretation of magnetic parameters has no single solution, it is necessary to compare them with other independent records, in order to evaluate the accumulation, distribution, preservation, and neoformation of the magnetic fraction, and support the paleoenvironmental interpretations derived from magnetic data [e.g. 16].

In this paper, we compare rock magnetic properties with geochemical data of a ca. 6 m long lacustrine sequence from Lago Verde near the Gulf of Mexico coast (Mexico). The aims of this study are: to identify the processes that determined and affected the sediment's magnetic properties, to construct a model of past environmental conditions based on these processes, and to compare our paleoenvironmental reconstructions and the archeological record of settlement patterns in the Gulf lowland area with the paleoclimatic shifts associated with the Classic Maya collapse, the Medieval Warm Period, and the Little Ice Age.

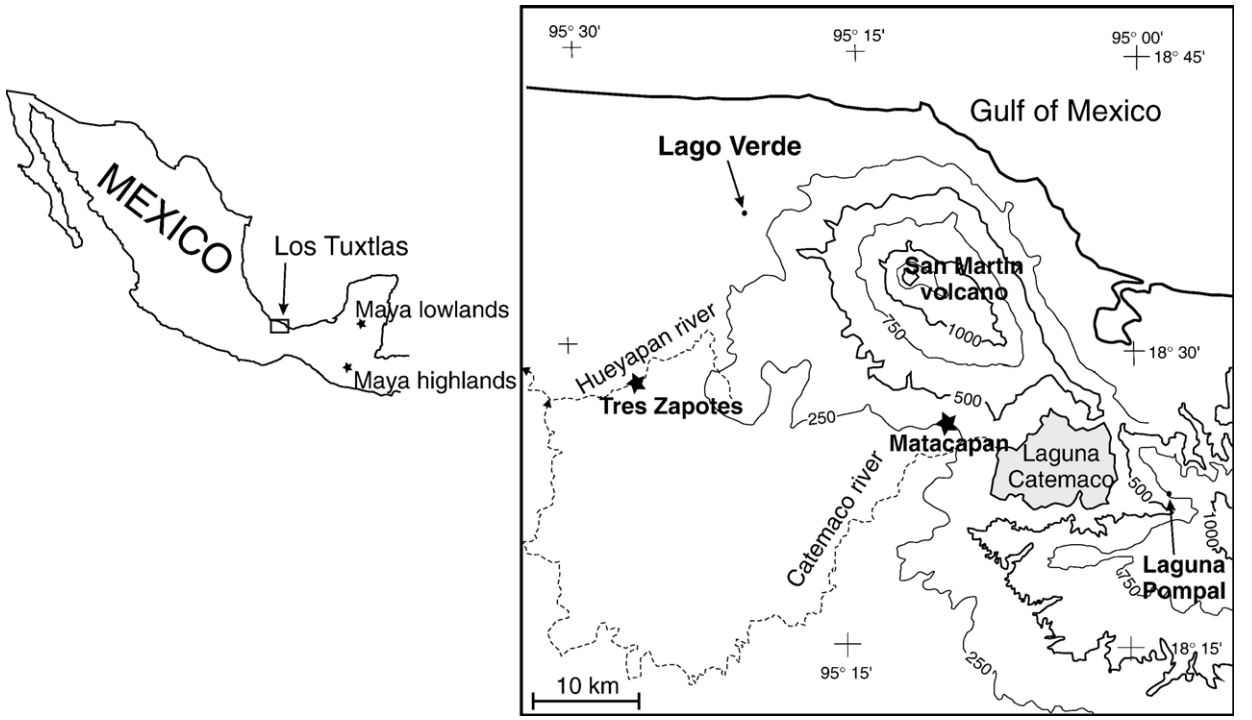

Fig. 1. Map of Lago Verde in the Los Tuxtlas area, Mexico. The location of San Martin volcano, the archeological sites of Tres Zapotes and Matacapan, the lakes Catemaco, Laguna Pompal and Lago Verde, and the Maya area, are shown.

2. Site description

The Los Tuxtlas volcanic field is located on the tropical coast of the Gulf of Mexico (Fig. 1). The main structure is the San Martin volcano, which had two historic pyroclastic events in A.D. 1664 and 1793 [17–19]. Today the Los Tuxtlas mountains lie at the northern limit of the tropical rainforest along the eastern coast of the American continent, a type of vegetation that has been severely modified over the last decades [20].

Lago Verde is one of seven phreatic explosion craters (maars) around the San Martin volcano with a permanent water body (Fig. 1). It is a semicircular, small, and shallow lake, ca. 4 m deep, nearly 0.8 km in diameter, and lies near the NE end of an elongated closed basin ca. 0.5 km^2 in size.

3. Methods

One Livingston-type piston core, 5.84 m long (in 1 m sections) was collected from the deepest part of the lake. The time scale of the sedimentary sequence was established by five ^{14}C AMS dates. All dates were determined on pollen concentrate, extracted from the sediment by a HCl, KOH and HF digestion method [21], and are summarized in Table 1. Dates were calibrated to calendar years using the Calib 5.0 program [22,23] with the IntCal04 data set [24]. Thirty pilot samples from representative stratigraphic horizons were collected into 8 cm^3 acrylic boxes, and preliminary measurements were performed at the Institute for Rock Magnetism (University of Minnesota). These preliminary analyses include mass-normalized low field susceptibility (χ), low temperature remanences, frequency-dependent susceptibility ($\chi fd\%$), hysteresis parameters and carbon content as discussed below.

The magnetic mineralogy of samples was characterized through the observation of Curie temperatures (Tc) or magnetic phase transitions. During heating, magnetic minerals lose their χ or remanence at specific temperatures [25], and some display crystallographic changes that aid in their identification [26–29]. Tc estimations were performed on a Bartington MS2WF furnace system in an atmosphere of air. This equipment did not have enough sensitivity to clearly define a Tc above 580 °C. Thermal demagnetization behavior of saturation remanence acquired at low temperatures (10 K) in a 2.5 Tesla (T) field, was measured while warming up to room temperature (300 K) in zero field in a Quantum Design MPMS SQUID magnetometer. Isothermal remanent magnetization (IRM) acquired in a forward field of 1 T and at backward fields of 100 and 300 mT were used to calculate S ratios. These ratios provide an indirect estimate of mineralogy, based on the magnetic coercivity distribution in samples, from low coercivity minerals (e.g. magnetite, high S), to high coercivity minerals (e.g. hematite or goethite, lower S). The magnetization acquired at 1 T was considered the saturation of IRM (SIRM). The ratio S was calculated as $S=(-IRM_{100,300}/SIRM)$. IRMs were imparted in an ASC pulse magnetizer and remanences were measured on a 2G 760-R cryogenic magnetometer.

The magnetic parameters dependent on the concentration of magnetic minerals are χ, SIRM, anhysteretic remanent magnetization (ARM) and saturation magnetization (Ms). Ti-magnetites have a higher intrinsic magnetization than hematite or goethite, and thus most concentration dependent parameters reflect mostly changes in these minerals [25]. As the diamagnetic (e.g. quartz, calcite), paramagnetic (e.g. Fe-bearing silicates and some sulphides) and ferrimagnetic (e.g. Ti-magnetites, pyrrhotite) mineral species account for χ, the ferrimagnetic susceptibility χf was calculated by subtracting the paramagnetic contribution χp, estimated from the high field slope in the hysteresis loops from χ. Additionally, 222 samples (8 cm^3) were later collected continuously along the core, and χ was measured using

Table 1
Radiocarbon dates from Lago Verde core VRUII-1 sediments, Los Tuxtlas, Veracruz, Mexico

Lab. code	Depth (m)	Sample type	δ13 C (o/oo)	Radiocarbon age (yr BP)	Calibrated date[1] (calendar years)	Sedimentation rate[2] (mm/yr)
Beta-176365	0.31	Pollen concentrate	−26.4	107.2+/−0.4	pMC★	2.52
AA47812	0.89	Pollen concentrate	−23	337+/−41	A.D. 1447− 1616	5.42
Beta-176366	1.72	Pollen concentrate	−18.8	490+/−40	A.D. 1413–1443	1.36
Beta-176367	2.66	Pollen concentrate	−27.4	1180+/−40	A.D. 779–891	1.85
AA47814	4.14	Pollen concentrate	−25.1	1978+/−36	36 B.C.–A.D. 64	

AA: Arizona
1: Calibration based on [22–24], 1s, Calib 5.0.1
2: Calculated from the two next dates.
★pMC=material was living within the last 50 years, reported result indicates an age of post 0 BP.

a MS2B Bartington system. ARM and SIRM were measured for 69 selected samples. ARM were imparted in a 50 μT bias field, superimposed on a peak alternating field of 100 mT in a Schonstedt GSD-1 demagnetizer. ARM and SIRM (at 1 T) were measured in a Molspin fluxgate magnetometer. Ms, remanent magnetization (Mr) and coercivity parameters Bcr, Bc were obtained from hysteresis loops (maximum field 1 T) measured with a Princeton Measurement Corporation Micro-vibrating Sample Magnetometer.

ARM is sensitive to single domain (SD, 0.1–0.05 μm) and small pseudo single domain (PSD, 1–0.1 μm) ferrimagnetic particles [25]. Since SIRM is rather insensitive to variations in grain size [30], it is common to estimate the relative abundance of SD grains by the ratio of ARM/SIRM [31]. SIRM/χ ratio displays high values where smaller, SD are present [32]. However, values of SIRM/χ > 70 kA/m are considered to be an indicator of the iron sulphide greigite [33]. $\chi fd\%$ is a proxy for the presence of SP particles [34]. $\chi fd\%$ was measured at 32 frequencies between 10 and 10,000 Hz at room temperature in 13 samples in a MPMS SQUID magnetometer, and calculated as $\chi fd\% = [(\chi 470\ \text{Hz} - \chi 4700\ \text{Hz})/\chi 470\ \text{Hz}]*100$, as these two frequencies are more often used.

In order to complement the magnetic mineralogy identification and the estimations of magnetic mineral concentrations, we used a combination of non-magnetic techniques. X-ray powder diffraction (XRD) analyses of selected bulk samples were performed in a Bucker-axs D8-Advance diffractometer and in a Phillips 1130/96 diffractometer. XRD, scanning electron microscopy observations (SEM) and energy dispersive X-ray analysis (EDAX) were carried out on magnetic separates. Magnetic grains were extracted using a continuous flux setup and a rare earth magnet device [35], and by using a Franz electromagnet at 0.1 A. Extraction succeeded only on the highest χ samples (from Units 3 and 4). Reflected light microscopy (RLM) was done on four samples from the main stratigraphic units.

Energy dispersive X-ray fluorescence analyses (XRF) for Fe, Ti and Zr were carried out on 26 of the pilot samples. Ti and Zr, which are immobile in most sedimentary environments and are not affected by diagenesis [36], provide information regarding the relative abundance of heavy minerals and consequently are a measure of detrital input in a basin. In contrast, Fe is highly mobile under most aqueous conditions. Comparison between magnetic properties and Ti, Zr and Fe may be useful for determining detrital input variations and posdepositional alterations.

Total carbon (TC) was measured in the pilot samples by combustion at 950 °C using a Coulometrics automated carbon dioxide coulometer. Total inorganic carbon (TIC) was measured as Carbon dioxide evolved by reaction with HCl from carbonates. Total organic carbon (TOC) was obtained by subtracting TC − TIC = TOC, and both TOC and TIC are expressed as percentages.

4. Results

4.1. Age model and stratigraphy

The ^{14}C dates are in agreement with the samples' stratigraphical position. The age of sediment at 0.30 m depth, dated by ^{137}Cs and ^{210}Pb is A.D. 1963 [37]. Sedimentation rates were calculated from linear regression between two dated horizons (Fig. 2). The time periods for the stratigraphic units described were estimated from sedimentation rates, and expressed in calendar years within the closest 5 years.

Four sedimentological units are identified (Fig. 2a). Unit 4 is composed of dark gray silt and black sand layers, with eleven tephras up to 1 cm in thickness (TV-TXV).

In Unit 3 subtle laminations, 1 to 3 mm in thickness, of dark gray and gray silt are present. Unit 2 consists of dark olive brown silt, with a sharp lower contact and an irregular upper contact. It has two tephra layers (TIV and TIII). In Unit 1, sediments older than A.D. 1963 are dark brown silt with carbon fragments. The top 0.30 m of sediment consists of very dark brown massive organic silt. It has two tephra layers (TII and TI), the later corresponds to the historical A.D. 1664 eruption of the San Martin volcano, according to its age [37].

4.2. Magnetic properties

The determination of magnetic mineral phases present in an assemblage of natural samples is critical to properly evaluate the significance of magnetic parameters, and consequently to correctly interpret the origin and transformations of these minerals, as well as the environment in which such changes occurred. We first present and discuss the results of magnetic mineralogy, and then the variations of magnetic concentration and grain size. The results of these magnetic analyses are then compared to the non-magnetic analyses.

4.2.1. Magnetic mineralogy

Tc measurements for Unit 4 tephras and lake sediments samples look similar. They show two drops in the heating curve χ (T), at 280 and near 580 °C, pointing to

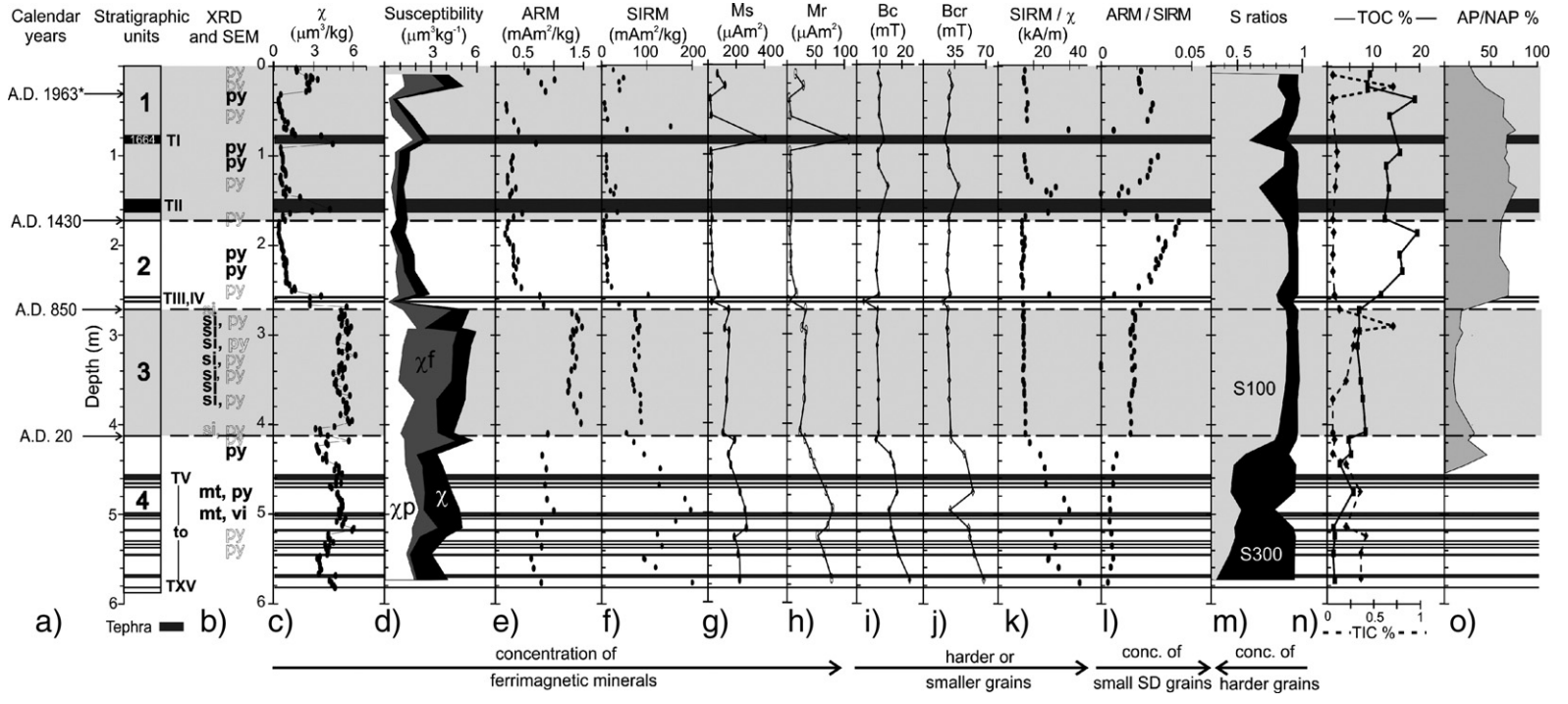

Fig. 2. a) Ages in calendar years (see Table 1), for stratigraphic units 1 to 4 of the Lago Verde core and position of tephras TI to TXV (dark gray shadow in the profiles). The A.D. 1963 date was obtained by ^{210}Pb and ^{137}Cs chronology [37]. b) Minerals detected by XRD and SEM analyses, si: siderite, mt: (Ti-)magnetite, py: pyrite, bold letters: positive identification, open letters: possible occurrence of minerals. c) Magnetic susceptibility (χ). d) χ expressed as bulk χ (black area), ferrimagnetic χf (gray area) and paramagnetic χp (white area). e) Anhysteretic remanent saturation (ARM). f) Saturation of isothermal remanent magnetization (SIRM). g) Saturation magnetization (Ms). h) Remanence magnetization (Mr). i) Coercivity (Bc) and j) coercivity of remanence (Bcr). χ, χf, ARM, SIRM Ms and Mr are proxies for the abundance of ferrimagnetic minerals. k) SIRM/χ is a proxy for the abundance of smaller particles or magnetically harder (higher coercivity) minerals. l) ARM/SIRM is a proxy for the relative abundance of fine (0.05–0.1 μm) single domain particles. m) S100 (gray area) and S300 (black area) ratios indicate the relative abundance of magnetically harder grains, such as hematite or gohetite. n) Total organic carbon (TOC, solid line) and total inorganic carbon (TIC, dashed line). o) Percentage of arboreal to non-arboreal pollen (AP/NAP) [46].

titanomagnetites or titanomaghemites with variable Ti content as the main magnetic carriers. It is only shown Tephra VII χ (T) curve (Fig. 3a). In Unit 3 dark gray sediment samples, warming χ (T) curves display a moderate increase in χ until ~250 °C, followed by a decay which is more pronounced close to 580 °C (Fig. 3b). In contrast, the χ (T) warming curves in the lighter, gray layers, show a sharp increase in χ between 350–500 °C, and a drop close to 580 °C (Fig. 3c). Most χ (T) curves are reversible in dark gray laminae, while they are non-reversible in gray layers. Iron sulphides, such as pyrite, phyrrotite or marcasite [38] or the Fe-carbonate siderite [28] may be responsible for the behavior observed in lighter layers. These alternatives will be further discussed.

The sediments from Units 1 and 2, are characterized by noisy χ (T) curves, mostly due to their low χ values. However, Ti-magnetites or Ti-maghemites seem to be the dominant magnetic minerals (Fig. 3d).

Low temperature demagnetization curves all show a similar behavior (Fig. 4). They display a steeper loss of remanence below 50 K, due to the thermal demagnetization of (super) paramagnetic minerals, and a subtle but recognizable drop near 120 K, the Verwey transition characteristic of magnetite. No magnetic iron sulphides, e.g. pyrrhotite or greigite, with characteristic Tc between 320–330 °C, and the low temperature transition at 34 K for pyrrhotite, were identified by the χ and remanence vs. temperature experiments.

Due to its low intrinsic magnetization, hematite is not detectable by magnetic measurements when present in low concentrations. High coercivity minerals (hematite, goethite) are not abundant in the sedimentary column, as S300 ratios are in most samples higher than 0.9. It is only in samples at 0.79 and 4.95 m S300 that ratios drop to nearly 0.8, suggesting a relative increment of high coercivity minerals in those samples (Fig. 2m) [25].

The iron forms detected by XRD are magnetite (in Unit 4), siderite (in Unit 3), and pyrite (confirmed in Units 1, 2 and 4, and suggested in Unit 3) (Fig. 2b). SEM observations on the magnetic extractions showed surrounded pitted grains of pure magnetite (Fig. 5a), and less altered crystals of Ti-magnetite (Fig. 5b), some with typical octahedral and skeletal forms (Fig. 5c). Partially

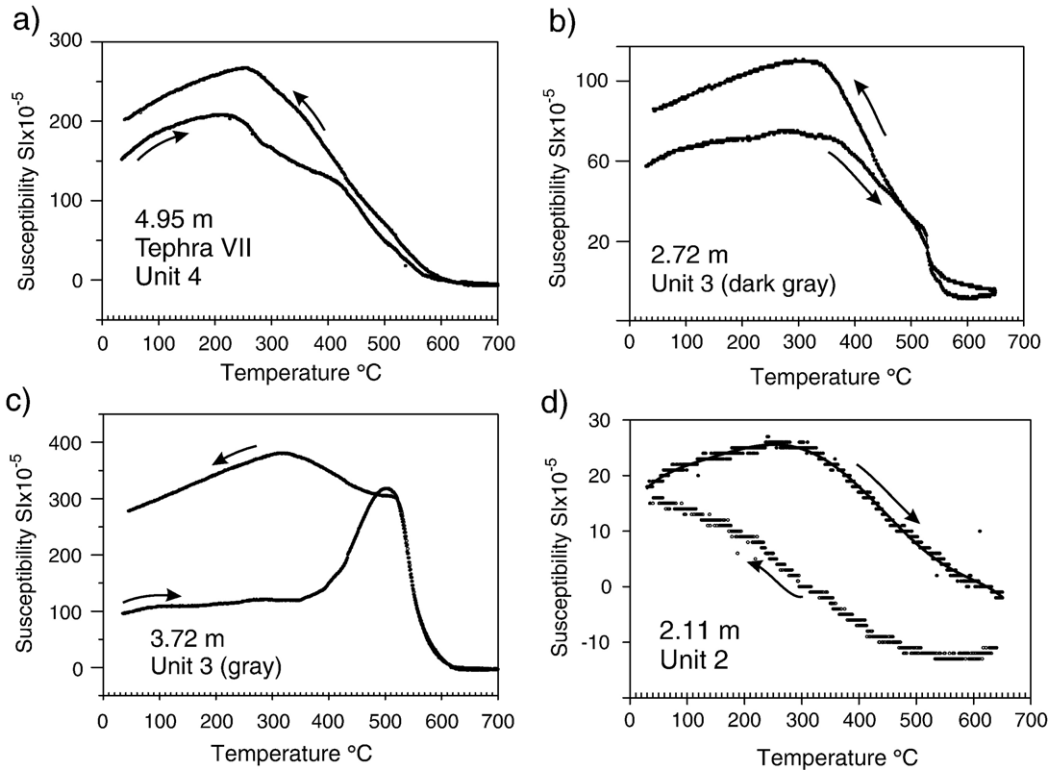

Fig. 3. χ vs. temperature curves. a) Tephra VII in Unit 4. Two magnetic phases are evident by change of the slope at 280 and 580 °C during heating, and a reversible curve during cooling. b) Dark gray sediments of Unit 3 have low initial χ, and a decay in χ between 300 and 650 °C. c) Gray sediments of Unit 3 have higher χ, and the formation of new minerals (magnetite) during heating begins at T>350 °C. d) Samples of low initial χ have noisy signal, although a decay in χ is observed between 300 and 650 °C.

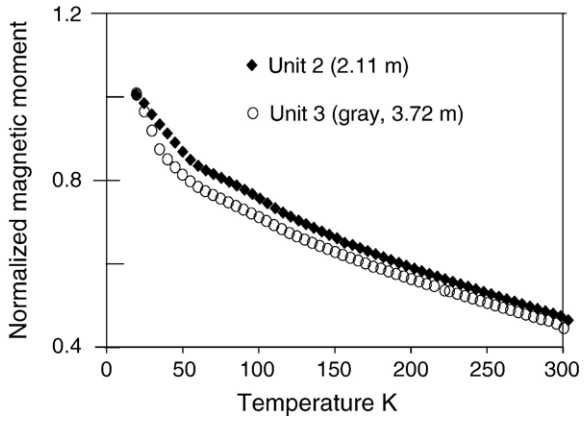

Fig. 4. Thermal demagnetization curves of low temperature IRM acquired at 10 K in 2.5 T field after cooling the samples from 300 K (room temperature). Remanences were measured while warming in zero field. Sample from gray laminae of Unit 3 (open circles) shows a steeper decay in remanence below 50 K than sample from Unit 2 (black diamonds), due to thermal unblocking of (super)paramagnetic particles. Both samples present a weak Verwey transition near 120 K, characteristic of magnetite.

hematized Ti-magnetites were observed by reflectance light microscopy (RLM) in samples from all units.

Pyrite occurs abundantly in Units 1 and 2, and in minor abundance in samples from Unit 4, as brass-yellow grains in spheroidal aggregates (Fig. 6a), some included in calcite, and partially replacing plant tissue (Fig. 6b). The observed spherules are commonly of bacterial origin [39]. The pyrite is thus of secondary, diagenetic origin in these sediments.

Greigite is difficult to recognize by its Tc, as this overlaps with transformations of other iron forms during heating [40]. In back-scattered electron images, it has been reported to have a brighter contrast than pyrite, although when greigite is very finely grained, its contrast can be darker than coarser grained pyrite. Such differences in size in Fe sulphide framboids that aid in differentiating greigite from pyrite were not seen in our samples' RLM observations, or in brightness contrast.

4.2.2. Magnetic concentration and grain size

Concentration-dependent parameters χ and ARM present similar variations throughout the core (Fig. 2). Unit 4 has a relatively high concentration of magnetic minerals, which decreases in the lower part and the topmost sediments of the unit (Fig. 2c,e). χ and ARM indicate that the highest concentration of magnetic minerals occurs in Unit 3 and in most tephras. Unit 2 and most of Unit 1 have the lowest concentration of magnetic minerals, and the sediments of the upper 0.40 m show an increase in χ (Fig. 2c). Based on the high field slope of the measured hysteresis curves, a diamagnetic contribution to χ is considered negligible in all samples. χ is mainly carried by ferrimagnetic minerals and χf is highest in Unit 3 sediments (Fig. 2d). However, χp contribute more than half of the χ signal in the lower part of Unit 4 (below 4.95 m) and part of Unit 2 and Unit 1

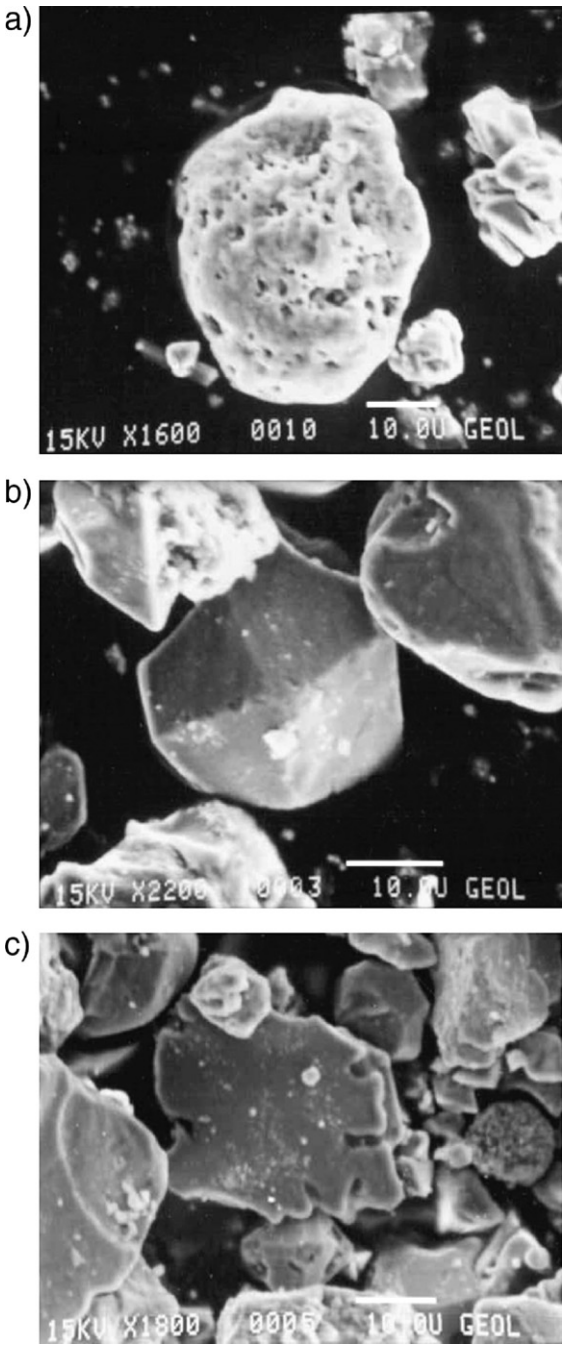

Fig. 5. Scanning electron microscopy (SEM) observations of minerals from Unit 4 (4.95 m depth). a) Rounded Ti free magnetite crystal showing pitted dissolution marks, and b) unaltered Ti-magnetite crystal. c) Skeletal Ti-magnetite.

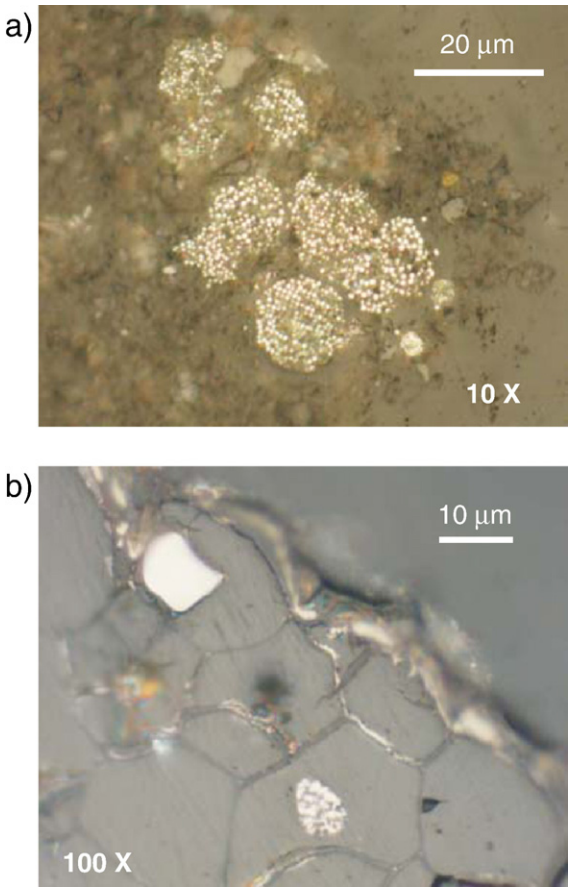

Fig. 6. Reflected light photomicrographs of samples. a) Pyrite framboids in a sample of Unit 4 (4.71 m depth). b) Plant tissue and spheroidal pyrite growing inside vacuoles and along their edges, from Unit 2 (2.11 m depth).

(2.30–0.35 m) (Fig. 2d). SIRM and Ms differ from χ and ARM, as Unit 4 displays the highest values in SIRM and MS, which are nearly twice as high as those values in Unit 3 (Fig. 2f,g). Except for some tephra layers, χ, SIRM and Ms are lowest in Units 2 and 1. SIRM/χ ratios are relatively high (>30 kA/m) in Unit 4 and in Tephras III, II and I, and their overlaying sediments in Units 2 and 1 (Fig. 2k). In opposition, ARM/SIRM (Fig. 2l) and S100 ratios (Fig. 2m) are low in those samples. The S100 (0.4–0.7) and S300 (>0.8) ratios suggest a component with intermediate coercivity, between 100 and 300 mT (Fig. 2m), which is also suggested by high Bc and Bcr (Fig. 2i, j). As ARM was acquired in a peak alternating field of 100 mT the ARM/SIRM ratio might be partly controlled by intermediate coercivity minerals. The differences above observed between magnetic parameters in the sequence are related not solely to changes in grain size distribution, but also to changes in magnetic mineralogy. A likely additional magnetic phase not identified in χ (T) or thermal demagnetization experiments, may be the iron sulphide greigite.

Higher concentrations of finer grains, are suggested by the incrementing upward trend of ARM/SIRM in Unit 2 and the lower part of Unit 1 (between 1.40 and 1.00 m), where S100 values are high (>0.8) (Fig. 2l,m). Very fine grains (SP) are scarce or absent, as χfd% are 2 to 3 % in samples measured throughout the core.

5. Discussion

The major mineral magnetic behavior changes are related to lithology, TOC content and the major elements Fe, Ti and Zr. In general terms, a higher concentration of magnetic minerals (e.g. χ) matches the highest values in Fe, Ti and Zr (Units 4 and 3, and sediments above 0.30 m in Unit 1) (Fig. 7), whereas the lowest concentrations in these elements coincide with zones of reduced magnetic mineral concentration (Unit 1 and 2) (Fig. 7). The correspondence in these variations suggests that the main changes in the concentration of magnetic minerals are related to detrital input. However, a comparison of χf and the conservative elements Ti and Zr reveals that χf varies approximately by a factor of 10, while Ti and Zr concentrations vary approximately by a factor of 2.5. This difference reveals that variations in χf are responding to an additional factor. The dissolution of ferrimagnetic minerals can cause the decrease in χf, at least in certain zones, as directly observed in magnetite grains at 4.95 m (Fig. 5a).

The use of combined magnetic and geochemical data for the unraveling of past environmental conditions has been applied in lake sediments [e.g. 14,41], where ratios of immobile elements (Ti, Zr) and Fe were utilized to detect posdepositional dissolution of magnetic minerals and changes in detrital input. In order to identify iron mineral alterations by redoximorphic processes, several ratios involving magnetic and non-magnetic data have been proposed, based on magnetic and geochemical data in marine sediments [42,43]. The authors of the present work are not aware of the application of such ratios in lake sediments.

The ratios that are sensitive to the dissolution of ferrimagnetic minerals (mainly Ti-magnetites) are $\chi p/\chi$, Fe/χ and χf/Ti [44,45]. $\chi p/\chi$ increases as the ferrimagnetic contribution to χ (χf) decreases, as $\chi p = \chi\text{total} - \chi f$. Higher ratios in $\chi p/\chi$ are directly related to increased dissolution of ferrimagnets as the removal of ferrimagnetic minerals leads to decreases in χ but leaves χp unaffected. Changes in Fe/χ identify the precipitation of paramagnetic Fe-bearing minerals (larger Fe), or the dissolution of ferrimagnetic minerals (smaller χ). In

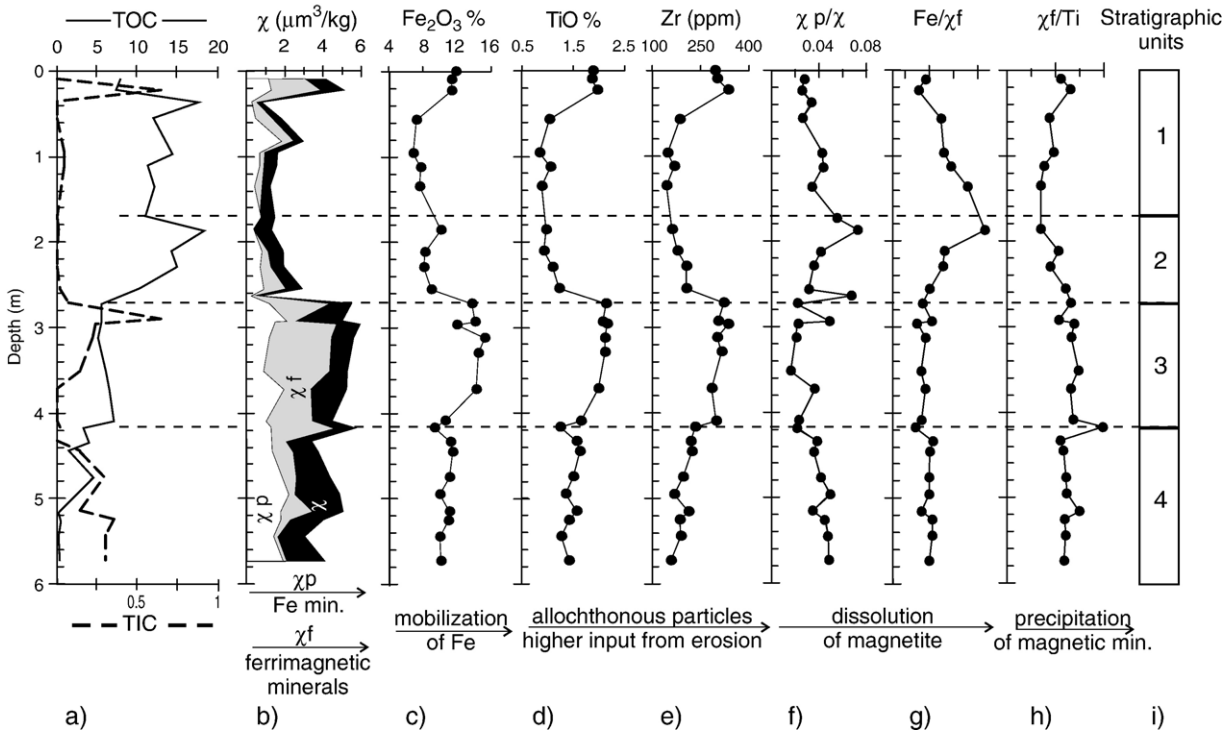

Fig. 7. Geochemical data and chemical–magnetic ratios. a) Total organic carbon (TOC, solid line) and total inorganic carbon (TIC, dashed line). b) Paramagnetic susceptibility (χp) is a proxy for the abundance of iron-bearing minerals, ferrimagnetic susceptibility (χf) is a proxy for the abundance of ferrimagnetic minerals. Both constitute the total susceptibility (χ). c) Fe, expressed as ferric oxide, is an indicator for mobilization and relocation of Fe. d) TiO and Zr (e), are proxies for detrital input to the lake. f) $\chi p/\chi$ and g) Fe/χf are proxies for dissolution of magnetite. h) χf/Ti is a proxy for magnetic mineral precipitation, as Ti only depends on detrital input. i) Stratigraphic units.

contrast, Fe/χf reveals the dissolution of ferrimagnetic minerals, as the denominator strictly measures ferrimagnetic minerals. An increase in χf/Ti is a proxy for the precipitation of magnetic minerals, as Ti is only present in primary detrital minerals (Ti-magnetites/Ti-maghemites). In order to reconstruct the evolution in environmental conditions that could affect the lake sedimentation we will now discuss these magnetic and non-magnetic results in more detail.

The pollen record of this core, currently under study [46], is used in this work as an independent proxy that supports the main conclusions. A detailed palynological analysis will be published elsewhere. The preliminary results are summarized in the arboreal/non-arboreal pollen (AP/NAP) curve (Fig. 2o). The pollen record starts at a depth of 4.4 m and no palynomorphs were recovered in the lower part of Unit 4.

5.1. Unit 4

The magnetic mineralogy of Unit 4 sediments is highly influenced by primary input of coarse MD Ti-magnetites or Ti-maghemites, as observed by SEM (Fig. 5), provided mainly by the abundant occurrence of tephras and the erosion of surrounding volcanic deposits. Pitted pure magnetite grains and unaffected or poorly affected Ti-magnetites, indicate the preferential dissolution of the still persistent pure magnetite, and the coarsening of magnetic grains by a selective dissolution of finer fraction (Fig. 5). Hematite, suggested by Tc measurements, is probably not abundant in the sediments according to S300 ratios and direct observations. Where organic matter (TOC) is relatively higher, paramagnetic pyrite is also present, as observed at depths of 4.33 and 4.75 m (Fig. 2n).

The dissolution of ferrimagnetic minerals in Unit 4, as indicated by the morphology of magnetites at 4.95 m depth (Fig. 5a), is not clearly observed in magnetic and geochemical ratios. $\chi p/\chi$ decreases from high to low values upwards in this unit and into Unit 3 (Fig. 7f), which indicates an upward decreasing dissolution of ferrimagnetic grains. However, the Fe/χf ratio decreases weakly upward and thus does not provide firm evidence for dissolution (Fig. 7g). An alternative explanation is

that dissolution is indeed weak, as magnetite still persists. Anoxic conditions are required for the dissolution of magnetite. Oxygen depletion by a rapid sedimentation of terrigenous flux into the basin in Unit 4 is not likely, as Ti and Zr are not particularly high, and lower than in the overlying Unit 3. However, the accumulation of several tephras can be an effective mechanism for rapid sedimentation. Diffusive fluxes of Fe released by dissolved oxides, combined with the presence of sulphur resulted in the neoformation of the observed pyrite framboids.

The relatively high coercivity and SIRM/χ in the lower part of Unit 4 could be due to the sulphide iron form of greigite [33,47]. This ferrimagnetic mineral is generally very finely grained (<1 μm), and occurs as a later stage of neoformation of diagenetic iron sulphides in anoxic sediments [47–49]. In sizes of 0.1 to 0.5 μm, it has been observed as fine grained crystals aggregates surrounding pyrite framboids [49].

Greigite precipitation may be related to the availability of sulphur, iron and organic matter, as the components needed for bacterial metabolism [41]. Relatively high Fe and moderate to low TOC may have been conditions that favored precipitation of greigite up to 4.20 m depth in Unit 4. When organic content increased, pyrite also precipitated.

Unit 4 sediments record the higher accumulation of tephras, suggesting enhanced volcanic activity, when compared to the rest of the core. The limnological conditions of this Unit are considered to have been anoxic reductive.

5.2. Unit 3

Higher χ, Fe, Ti and Zr and moderately high TOC are the common characteristics of Unit 3. The highest TIC values occur in the upper part of the unit. The paramagnetic iron carbonate siderite, $FeCO_3$, is confirmed by XRD where TIC is higher. The magnetic properties of the dark gray layers are dominated by magnetite. In the gray layers, the sharp increase in χ at temperatures >350 °C (Fig. 3c) is due to the formation of new magnetic mineral phases, which appeared to be magnetite. Conversion of paramagnetic minerals, including clays and siderite, into magnetites is probably responsible for this behavior. Low temperature demagnetization experiments showed the steepest warming curves between 10–50 K, which indicate a larger SP or paramagnetic content, and a weak Verwey transition of magnetite (Fig. 4). Those curves did not show the rapid drops in magnetization between 30 and 40 K found in marine siderite [28], as the presence of more strongly magnetic minerals, such as magnetite and Ti-magnetite/Ti-maghemite, or the poor crystallinity of authigenic siderite, may shadow the low temperature signature.

High χf, which is even higher than in the tephras, together with the high concentrations of Ti and Zr, and a relatively high sedimentation rate (1.85 mm/yr), indicate higher erosion from the catchment.

High Fe and χf/Ti indicate that Fe mobilization by reductive conditions did not significantly deplete the iron content of these sediments (Fig. 7c and h), as both ferrimagnetic and also paramagnetic minerals occur.

Unit 3 sediments, dated between A.D. 20–850, were deposited in an environment of moderate organic matter deposition (TOC) with relatively high inorganic carbon content. Available organic carbon and oxygen depletion in porous spaces by a rapid flux of sediments into the basin led to anoxic conditions. The available TIC favored the precipitation of paramagnetic siderite, which forms in anoxic, non-sulphuric conditions [50]. The suggested presence of pyrite by XRD, which precipitates in anoxic sulphuric environments, may have been formed as a result of variations in sulphide availability.

An increase in water temperature or pH could cause the release of CO_2 and the precipitation of carbonates [51]. A rise in pH could be related to higher productivity in the lake [52], and consequently higher organic matter accumulation in the sediments, anoxia and the precipitation of carbonates occur. However, TOC remains constant along Unit 3 while TIC increases upwards. We consider that the increase in TIC is linked to an increase in temperature and evaporation, which may have resulted in a lowering of the lake level. Higher concentrations of siderite in gray layers may indicate periodical increases in water temperature or decreases in the precipitation/evaporation balance, and these periodical changes caused the observed banding in sediments. Additional evidence of anoxia is the absence of disturbance through bioactivity in the subtle but recognizable banding of these sediments. The pollen record is dominated by herbaceous disturbance elements, such as *Ambrosia*, *Acacia*, Asteraceae and Poaceae. This pollen association is consistent with the scenario of an open vegetation cover, which allowed runoff erosion, and relatively dry conditions.

5.3. Unit 2

The magnetic and non-magnetic characteristics of sediments in Unit 2 are very different from those of the underlying Unit 3. The differences found are recorded before the deposition of tephras TIII and TIV, and are related to changes in the sedimentation regime rather

than a volcanic effect. In Unit 2 sediments, no pure (Ti free) magnetite was observed by microscopy.

Based on the observed high values of Fe/χf, dissolution of magnetite is likely to have occurred in Unit 2 sediments (Fig. 7g). This Unit, dated between A. D. 850–1430, is characterized by an upward increase of TOC content, the presence of paramagnetic pyrite confirmed by XRD, and by low χf/Ti values (Fig. 7). The low content of Ti and Zr, and the lowest calculated sedimentation rates (~1.36 mm/yr), indicate low detrital input.

The upward increase in the relative abundance of fine SD grains (higher ARM/SIRM) while dissolution of magnetite takes place is unexpected, as finer grains with larger surface/volume ratios are dissolved at higher rates. This implies that the SD grains are inclusions in silicates, protected from reduction.

The dissolution of iron oxides and the neoformation of pyrite occurred in anoxic sulphidic conditions, favored by high organic matter concentrations. The upward increasing trends in $\chi p/\chi$, Fe/χf, TOC and ARM/SIRM in this unit, opposite to χ and χf/Ti, suggest an increasing dissolution of magnetite and a reduction in grain size. Anoxic conditions in this unit are due to an increase in productivity in deeper water, which implies higher lake levels and more diluted water. The pollen record also shows conditions different from those in Unit 3. Arboreal pollen increases from 25 to 75 % at the base of Unit 2, which is characterized by tropical pioneer taxa (*Cecropia* and *Trema*) and rain forest (Moraceae, *Ficus*, *Aphanante monoica*) elements. The recorded expansion of the forest coincides with our interpretation of low runoff erosion and higher lake levels, which together indicate the end of dry conditions and increased precipitation in the region.

5.4. Unit 1

A change in texture characteristics and lower TOC are the main differences observed between sediments of Unit 2 and Unit 1. Tephras II (1.56 m) and I (0.85 m, A.D. 1664) seem to have altered the environment, providing new rock forming minerals, and leading to increases in χ in Unit 1 (Fig. 2c). After the deposition of the tephras, conditions gradually returned to their previous state, as is observed in most parameters. Greigite is probably present at a depth of around 1.40 m and above Tephra I, as there are slight increases in SIRM/χ and Bc and Bcr, and a weak decrease in S ratios (Fig. 2). Dissolution of magnetite in Unit 1 decreases upwards, as is shown by the progressive lowering of $\chi p/\chi$, and Fe/χf ratios, and the increase of χf/Ti (Fig. 7f, g, h). The decrease in TOC is probably the factor that caused less favorable conditions for magnetite dissolution. The upper 0.35 m, the last 40 years, are characterized by high χ, Fe, Ti and Zr, lower TOC and a peak in TIC, which suggest a recent trend to higher erosion rates, related to the modern destruction of the rainforest [37]. Pyrite is still present in sediments of Unit 1. An expansion of the rain forest, abundant palms and mesophyllous forest taxa in higher altitudes are recorded in the lower section of Unit 1 (A.D. 1430–1960). In the upper 0.35 m the pollen record is characterized by the dominance of herbaceous taxa, with abundant charcoal particles and cultivated *Zea mays* pollen, revealing human impact in the region.

6. Implications for archeological and paleoclimatic records

The major archeological centers nearest to Lago Verde are Tres Zapotes (19 km SW), and Matacapan (34 km SE), which were occupied since the Early Formative period ca. 1500 B.C. (Fig. 8) [5,53]. Archeological research at Tres Zapotes indicates the distribution of fertile soils along the Hueyapan river valley and the easy access to basalt outcrops required to produce a variety of tools and products, nucleated residential settlements [54]. Settlements in Matacapan depended on the availability of Catemaco river valley soils for agriculture [5]. Decline in soil fertility, flood events in the lowlands, local social conflicts and ash fall from volcanic vents are the argued causes for shifts in settlement patterns and the abandonment of these sites several times between the beginning of Terminal Formative (ca. A.D. 100) and end of the Late Classic (ca. A. D. 900–1000) [5,55,56]. A synthesis of the inferred environmental conditions, settlement patterns, ash falling events and some cultural characteristics for both sites are shown in Fig. 8. Between A.D. 100 and A.D. 300 population decreases and the partial abandonment of the sites have been documented. Large population growth occurred between A.D. 300 and A.D. 600–650, followed by a decline in occupation and a final abandonment around A.D. 1000. According to some authors [5,56], the general drop in population from the Terminal Formative to the Post-classic in the Olmec area may have been due to progressive declines in soil fertility.

The pollen record of Laguna Pompal (Fig. 1) documents a history of occupation before 2880 B.C. Between 650 B.C. and A.D. 725 forest clearance, very shallow lake levels, a negative precipitation balance and drier conditions are recorded [9]. Following this dry phase, a rapid recovery of the forest is documented, and by A.D. 1550, a second period of agriculture and forest

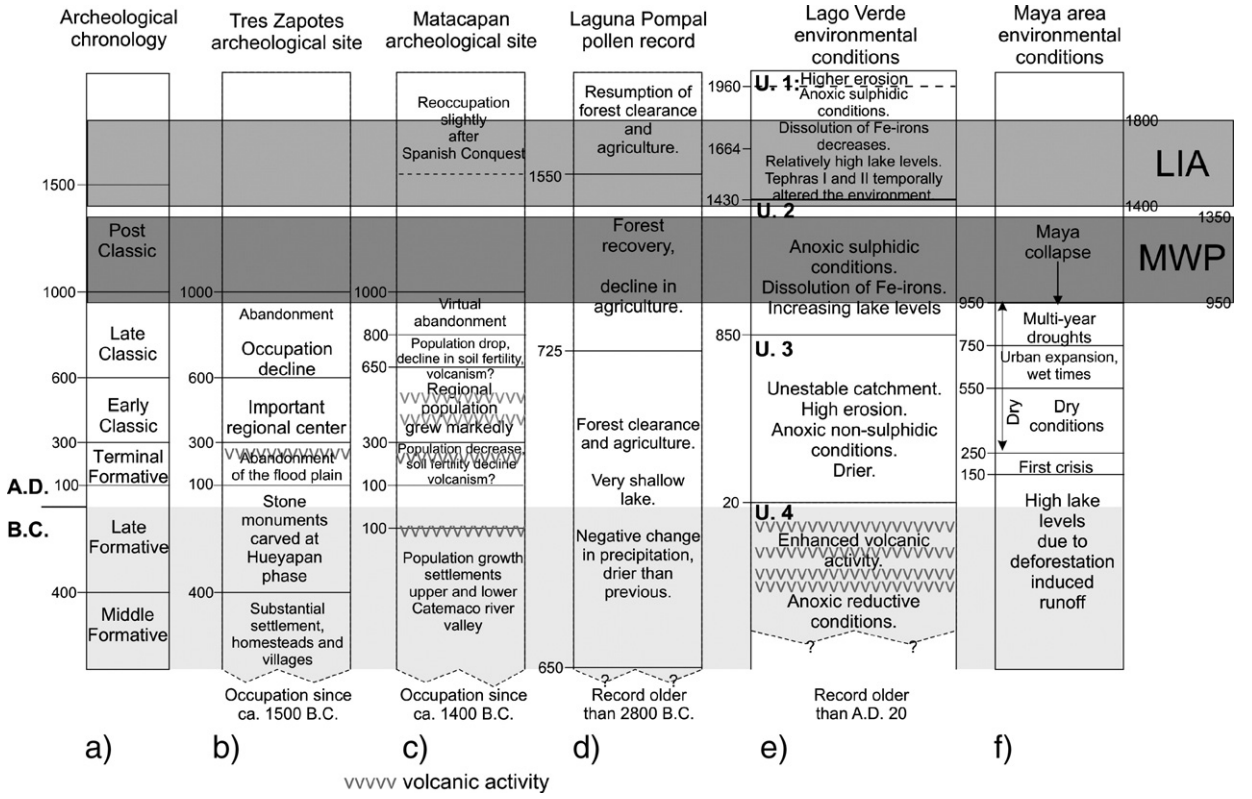

Fig. 8. Comparison between the archeological record and paleoenvironmental reconstructions from the Gulf lowlands, and the major paleoclimatic events inferred in the Maya area. a) Archeological chronology for Gulf lowlands [56]. Ages expressed as calendar years. Faint shaded area indicates B.C. times. b) Settlement history for the archeological sites of Tres Zapotes [53], and (c) Matacapan [5,55]. d) Pollen-based environmental reconstruction for Laguna Pompal [9]. e) Inferred paleoenvironmental conditions for Units 1 to 4 in Lago Verde (this study). f) Major climatic disturbances and related occupation changes in the Maya area [1,57]. Medieval Warm Period (MWP) and Little Ice Age (LIA) climatic events.

disturbance is linked to Spanish colonization (Fig. 8). Although the beginning of dry conditions in Lago Verde is recorded to have happened later than in Laguna Pompal, the end of the dry phase coincides in both sites within 150 years. The higher lake levels and the low runoff erosion recorded in Lago Verde after ca. A.D. 850 are contemporary to the recovery of the forest and the decline in agriculture inferred in Laguna Pompal (Fig. 8). The renewal in agriculture after the Spanish Conquest documented in Laguna Pompal (after ca. A.D. 1550) does not have a clear correspondence in Lago Verde's magnetic and geochemical record. In Lago Verde, major differences in magnetic and geochemical parameters are only recorded after A.D. 1963, when exacerbated deforestation led to increased erosion.

In Lake Salpeten in the southern Maya area, high lake levels are inferred from increased runoff due to deforestation between 400 B.C.–A.D. 150 [3]. Hodell and co-authors [1,57] have suggested that recurrent patterns of drought played an important role in Maya civilization. Between A.D. 150–250, the first historical crisis and the Preclassic abandonment of major cities in the lowlands coincide with inferred dry conditions in the Cariaco basin sediments (Venezuela) [4]. Favorable relatively wet times from A.D. 550 to 750 are suggested to have resulted in an expansion of the population, operating at the limits of environmental capacity, which ended in multiyear drought events between A.D. 750–950 [4]. In the northern Maya area, in Lake Punta Laguna, dry conditions are suggested after A.D. 250 and until ca. A.D. 1000 [2], and in Lake Chichancanab a 200 year drought is recorded ca. A.D. 800 [1,57]. These dry periods are associated with climatic conditions that diminished rainfall, as they prevented the Inter-tropical Convergence Zone from penetrating northern regions [4]. The general pattern of dry conditions in the Maya area corresponds to the relatively dry environments inferred for the Gulf lowlands in Lago Verde and Laguna Pompal.

Records of multi-centennial warming and cooling periods over the past 1000 years in marine sediments of the Santa Barbara basin (off California) [58] and the Gulf of California [59] are correlated to the Medieval Warm

Period (MWP) (A.D. 950–1350) and the Little Ice Age (LIA) (A.D. 1400–1800). In central Mexico, glacial chronology records an advance contemporary to LIA, which implies cold but also moist conditions [60]. In the marine sediments of the Cariaco basin, higher precipitation is recorded at the beginning of the MWP and has a large decreasing trend during LIA [4]. The higher lake levels interpreted in our record of Lago Verde after A.D. 850 correlate to the increase in precipitation during the MWP, and suggest the continuity of relatively moist conditions during the LIA, in agreement with the glacial chronology data. Higher erosion is documented for the last 40 years, when cattle ranching and other agroindustries raised in the region [37].

7. Conclusions

The mineral magnetic and geochemical parameters and ratios for the sedimentary record of Lago Verde provide a record of past environmental conditions. The use of combined magnetic and geochemical data allowed a more detailed reconstruction of past environmental conditions. The processes that affected sedimentation were dominated by the ash falling from unidentified vents in the San Martin volcanic complex, changes in redox conditions, the availability of organic matter and inorganic carbon that conditioned the dissolution and precipitation of Fe-bearing minerals, and variations in detrital input. The environmental variations interpreted in this work from the magnetic mineral and geochemical records are consistent with independent proxy data from the pollen record. The relatively dry conditions identified in Gulf lowland area between the Late Formative and the Late Classic periods agree with the paleoclimatic conditions linked to the collapse of Mayan civilization. Higher lake levels in Lago Verde and the forest recovery in Laguna Pompal broadly coincide with the increased precipitation documented during the Medieval Warm Period after A.D. 950 in the northern tropical and subtropical regions of American continent. For the Little Ice Age after A.D. 1350, relatively moist conditions in records for the Gulf lowlands are in concordance with the glacial advances recorded in central Mexico, rather that with a large decrease in precipitation as recorded in the Cariaco basin. Erosion in Lago Verde basin increased in the last 40 years as result of anthropic activities.

Acknowledgements

We thank the staff members of the Limnological Research Center and the Institute for Rock Magnetism (IRM), University of Minnesota, for their kind assistance in the initial description of cores and TC/TIC analyses, and magnetic measurements. The IRM is founded by the Earth Sciences Division of the National Science Foundation and the W. M. Keck Foundation. The study was founded by CONACYT G28528T, and DGAPA IN107902 projects. S. Angeles and M. Reyes assisted in SEM observations. L. Baños and T. Pi in XRD. L. Rivas helped in RLM identifications. R. Lozano made XRF analysis. We also thank A. Gonzalez and R. Robledo for coring, T. Hernandez for technical assistance and S. Sosa for pollen extraction. Particular thanks go to A. Daneels for archeological discussion. Authors thank Dr. C. Geiss and an anonymous reviewer whose comments greatly improved the manuscript.

References

[1] D.A. Hodell, J.H. Curtis, M. Brenner, Possible role of climate in the collapse of Classic Maya civilization, Nature 375 (1995) 391–394.
[2] J.H. Curtis, D.A. Hodell, M. Brenner, Climate variability on the Yucatan Peninsula (Mexico) during the past 3500 years, and implications for Maya cultural evolution, Quat. Res. 46 (1996) 37–47.
[3] M.F. Rosenmeier, D.A. Hodell, M. Brenner, J.H. Curtis, A 4000-year lacustrine record of environmental change in the southern Maya lowlands, Peten, Guatemala, Quat. Res. 57 (2002) 183–190.
[4] G.H. Haugh, D. Günther, L.C. Peterson, D.M. Sigman, K.A. Hughen, B. Aeschlimann, Climate and the collapse of Maya Civilization, Science 299 (2003) 1731–1735.
[5] R.S. Santley, P.J. Arnold III, Prehispanic settlement patterns in the Tuxtlas mountains, southern Veracruz, Mexico, J. Field Archaeol. 23 (2) (1996) 225–249.
[6] J. Valenzuela, Las exploraciones efectuadas en Los Tuxtlas, Veracruz, Anales del Museo Nacional de Arqueologia, Historia y Etnologia, Mexico 3 (1945) 83–107.
[7] M.D. Coe, Archaeological synthesis of southern Veracruz and Tabasco, in: R. Wauchope (Ed.), Archaeology of Southern Mesoamerica, Part 2, Handbook of Middle American Indians, vol. 3, University of Texas Press, Austin, 1965, pp. 679–715.
[8] R. Byrne, S. Horn, Prehistoric Agriculture and Forest Clearance in the Sierra de los Tuxtlas, Veracruz, Mexico, Palynology 13 (1989) 181–193.
[9] M. Goman, R. Byrne, A 5000-year record of agriculture and tropical forest clearance in the Tuxtlas, Veracruz, Mexico, Holocene 8 (1) (1998) 83–89.
[10] B.K. Reinhardt, Volcanology of the younger volcanic sequence and volcanic hazards study of the Tuxtla Volcanic Field, Veracruz, Mexico, Unpublished Master's Thesis, Department of Geology, Tulane University, 1991.
[11] A. Sluyter, Regional Holocene records of the human dimension of global change: sea-level and land-use change in prehistoric Mexico, Glob. Planet. Change 14 (1997) 127–146.
[12] C. Siebe, M. Abrams, M.F. Sheridan, Major Holocene block-and-ash fan at the western slope of ice-capped Pico de Orizaba, México: implications for future hazards, J. Volcanol. Geotherm. Res. 59 (1993) 1–33.
[13] M. Heimo, Prehispanic wetland agriculture south of Laguna Mandinga, Veracruz, Mexico: testing postulations of water

management and agricultural intensification, Unpublished Master's Thesis, Department of Geography, University of British Columbia, Vancouver, Canada, 1998.
[14] J.G. Rosenbaum, R.L. Reynolds, D.P. Adam, J. Drexler, A.M. Sarna-Wojcicki, G.C. Whitney, Record of middle Pleistocene climate change from Buck Lake, Cascade Range, southern Oregon— evidence from sediment magnetism, trace-element geochemistry, and pollen, GSA Bull. 108 (10) (1996) 1328–1341.
[15] B.A. Maher, R. Thompson, Quaternary Climates, Environments and Magnetism, Cambridge University Press, 1999.
[16] C.E. Geiss, S.K. Banerjee, A multi-parameter rock magnetic record of the last glacial–interglacial paleoclimate from south–central Illinois, USA, Earth Planet. Sci. Lett. 152 (1997) 203–216.
[17] S.A. Nelson, E. Gonzalez-Caver, Geology and K–Ar dating of the Tuxtla Volcanic Field, Veracruz, Mexico, Bull. Volcanol. 55 (1992) 85–96.
[18] S.A. Nelson, E. Gonzalez-Caver, T. Kurtis Kayser, Constraints on the origin of alkaline and calc-alkaline magmas from the Tuxtla Volcanic Field, Veracruz, Mexico, Contrib. Mineral. Petrol. 122 (1995) 191–211.
[19] R.S. Santley, S.A. Nelson, B.K. Reinhardt, C.A. Pool, P.J. Arnold, When day turned to night. Volcanism and the archeological record from the Tuxtla mountains, southern Veracruz, Mexico, in: G. Bawden, R.M. Reycraft (Eds.), Environmental Disaster and the Archaeology of Human Response, Anthropological Papers, vol. 7, Maxwell Museum of Anthropology, 2000, pp. 143–162.
[20] R. Dirzo, M.C. Garcia, Rates of deforestation in Los Tuxtlas, a neotropical area in southeast Mexico, Conserv. Biol. 6 (1) (1992) 84–90.
[21] T.H. Brown, D.E. Nelson, R.W. Mathewes, J.S. Vogel, J.R. Southon, Radiocarbon dating of pollen by accelerator mass spectrometry, Quat. Res. 32 (1989) 205–212.
[22] M. Stuiver, P.J. Reimer, Extended ^{14}C data base and revised Calib 3.0 ^{14}C calibration program, Radiocarbon 35 (1993) 215–230.
[23] M. Stuiver, J.P. Reimer, R.W. Reimer, CALIB 5.0 program and documentation (2005) http://calib.qub.ac.uk/calib/calib.html.
[24] P.J. Reimer, M.G.L. Baillie, E. Bard, A. Bayliss, J.W. Beck, C.J.H. Bertrand, P.G. Blackwell, C.E. Buck, G.S. Burr, K.B. Cutler, P.E. Damon, R.L. Edwards, R.G. Fairbanks, M. Friedrich, T.P. Guilderson, A.G. Hogg, K.A. Hughen, B. Kromer, F.G. McCormac, S.W. Manning, C.B. Ramsey, R.W. Reimer, S. Remmele, J.R. Southon, M. Stuiver, S. Talamo, F.W. Taylor, J. van der Plicht, C.E. Weyhenmeyer, IntCal04 Terrestrial radiocarbon age calibration 26–0 ka BP, Radiocarbon 46 (2004) 1029–1058.
[25] C.P. Hunt, B.M. Moskowitz, S.K. Banerjee, Magnetic properties of rocks and minerals, Rock Physics and Phase Relations, A Handbook of Physical Constants, AGU Reference Shelf, vol. 3, 1995, pp. 189–204.
[26] E.J. Verwey, P.W. Haayman, F.C. Romeijn, Physical properties and cation arrangements of oxides with spinel structure, J. Chem. Phys. 15 (1947) 181–187.
[27] F.J. Morin, Magnetic susceptibility of α-Fe_2O_3 and α-Fe_2O_3 with added titanium, J. Phys. 3 (1950) 819–820.
[28] B.A. Housen, S.K. Banerjee, B.M. Moskowitz, Low-temperature magnetic properties of siderite in marine sediments, Geophys. Res. Lett. 23 (1996) 2843–2846.
[29] P. Rochette, G. Fillion, J.L. Mattei, M.J. Dekkers, Magnetic transition at 30–34 Kelvin in pyrrhotite: insight into a widespread occurrence of this mineral in rocks, Earth Planet. Sci. Lett. 98 (1990) 319–328.
[30] M.E. Evans, F. Heller, Environmental Magnetism, Principles and Applications of Enviromagnetics, Academic Press, San Diego, 2003.
[31] J.W. King, S.K. Banerjee, J.A. Marvin, Ö. Özdemir, A comparison of different magnetic methods for determining the relative grain size of magnetite in natural materials: some results from lake sediments, Earth Planet. Sci. Lett. 59 (1982) 404–419.
[32] F. Heider, A. Zitzelsberger, F. Fabian, Magnetic susceptibility and remanent coercive force in grown magnetite crystals from 0.1 μm to 6 mm, Phys. Earth Planet. Inter. 93 (1996) 239–256.
[33] J.W.E. Fassbinder, H. Stanjek, Magnetic properties of biogenic soil greigite (Fe_3S_4), Geophys. Res. Lett. 21 (1994) 2349–2352.
[34] H.U. Worm, On the superparamagnetic-stable single domain transition for magnetite, and frequency dependence of susceptibility, Geophys. J. Int. 133 (1998) 201–206.
[35] N. Petersen, T. von Dobeneck, H. Vali, Fossil bacterial magnetite in deep-sea sediments from the South Atlantic Ocean, Nature 320 (1986) 611–615.
[36] J. Thomson, I. Jarvis, D.R.H. Green, D. Green, Oxidation fronts in Madeira abyssal plain turbidites: persistence of early diagenetic trace-element enrichments during burial, Site 950, in: P.P.E. Weaver, H.U. Schmincke, J.V. Firth, W. Duffield (Eds.), Proceedings ODP Scientific Results, vol. 157, College station, Texas, 1998, pp. 559–571.
[37] M. Caballero, G. Vazquez, S. Lozano-Garcia, A. Rodriguez, S. Sosa-Najera, A.C. Ruiz-Fernandez, B. Ortega, Present limnological conditions and recent (ca. 340 yr) palaeolimnology of a tropical lake in the Sierra de Los Tuxtlas, Eastern Mexico, J. Paleolimnol. 35 (2006) 83–97.
[38] C.E. Geiss, The development of rock magnetic proxies for paleoclimatic reconstructions, Unpublished Ph.D. Thesis, University of Minnesota,1999.
[39] S.S. Augustithis, Atlas of the Sphaeroidal Textures and Structures and Their Genetic Significance, Theophrastus Pubs., Athens, Greece, 1982.
[40] F. Heider, J.M. Bock, I. Hendy, J.P. Kennett, J. Matzka, J. Schneider, Latest Quaternary rock magnetic record of climatic and oceanic change, Tanner basin, California borderland, GSA Bull. 113 (3) (2001) 346–359.
[41] R.L. Reynolds, J.G. Rosenbaum, P. van Metre, M. Tuttle, E. Callender, A. Goldin, Greigite (Fe_3S_4) as an indicator of drought—the 1912–1994 sediment magnetic record from White Rock Lake, Dallas, Texas, USA, J. Paleolimnol. 21 (1999) 193–206.
[42] S.G. Robinson, J.T.S. Sahota, F. Oldfield, Early diagenesis in North Atlantic abysal plain sediments characterized by rock magnetic and geochemical indices, Mar. Geol. 163 (2000) 77–107.
[43] T. von Dobeneck, J. Funk, Integrated rock magnetic and geochemical proxies for iron mineral dissolution and precipitation in marine sediments based on single sample and new split core scanning techniques, in: L. Sagnotti, A.P. Roberts (Eds.), International Symposium on Fundamental Rock Magnetism and Environmental Applications, Quaderni di Geofisica, vol. 26, 2002, pp. 183–185, Extended abstracts.
[44] J.A. Funk, T. von Dobeneck, A. Reitz, Integrated rock magnetic and geochemical quantification of redoxomorphic iron mineral diagenesis in late Quaternary sediments from the Equatorial Atlantic, in: G. Wefer, S. Mulitza, V. Ratmeyer (Eds.), The South Atlantic in the Late Quaternary: Reconstruction of Material Budgets and Current Systems, Springer-Verlag, Berlin, 2004, pp. 237–260.
[45] J.A. Funk, T. von Dobeneck, T. Wagner, S. Kasten, Late Quaternary sedimentation and early diagenesis in the Equatorial

Atlantic ocean: patterns, trends and processes deduced from rock magnetic and geochemical records, in: G. Wefer, S. Mulitza, V. Ratmeyer (Eds.), The South Atlantic in the Late Quaternary: Reconstruction of Material Budgets and Current Systems, Spinger-Verlag, Berlin, 2004, pp. 461–497.

[46] M.S. Lozano-Garcia, S. Sosa-Najera, M. Caballero, Late Holocene pollen record of Lago Verde in the tropical lowland of the Mexican Gulf coast, in: J.L. Ubera (Ed.), XI International Palynological Congress Proceedings Universidad de Cordoba, Spain, Polen, vol. 14, 2004, p. 548.

[47] A.P. Roberts, Magnetic properties of sedimentary greigite (Fe_3S_4), Earth Planet. Sci. Lett. 134 (1995) 227–236.

[48] A.P. Roberts, G.M. Turner, Diagenetic formation of ferrimagnetic iron sulphide minerals in rapidly deposited marine sediments, South Island, New Zealand, Earth Planet. Sci. Lett. 115 (1993) 257–273.

[49] W.T. Jiang, C.S. Horng, A.P. Roberts, D.R. Peacor, Contradictory magnetic polarities in sediments and variable timing of neoformation of authigenic greigite, Earth Planet. Sci. Lett. 193 (2001) 1–12.

[50] R.A. Berner, A new geochemical classification of sedimentary environments, J. Sediment. Petrol. 51 (1981) 359–365.

[51] R.G. Wetzel, Limnology, Lake and River Ecosystems, Academic Press, San Diego, 2001.

[52] W. Dean, A 1500-year record of climatic and environmental change in Elk Lake, Clearwater County, Minnesota II: geochemistry, mineralogy, and stable isotopes, J. Paleolimnol. 27 (2002) 301–319.

[53] C.A. Pool, Introduction, in: C.A. Pool (Ed.), Settlement Archaeology and Political Economy at Tres Zapotes, Veracruz, Mexico, The Cotsen Institute of Archaeology, Monograph, vol. 50, University of California, Los Angeles, 2003, pp. 1–6.

[54] C.A. Pool, Centers and peripheries, in: C.A. Pool (Ed.), Settlement Archaeology and Political Economy at Tres Zapotes, Veracruz, Mexico, The Cotsen Institute of Archaeology, Monograph, vol. 50, University of California, Los Angeles, 2003, pp. 90–98.

[55] R.S. Santley, A consideration of the Olmec Phenomenon in the Tuxtlas: Early Formative settlement pattern, land use, and refuse disposal at Matacapan, Veracruz, Mexico, in: T.W. Killion (Ed.), The Gardens of Prehistory: the Archaeology of Settlement Agriculture in Greater Mesoamerica, University of Alabama Press, Tuscaloosa, 1992, pp. 150–183.

[56] C.A. Pool, M.A. Ohnersorgen, Archaeological Survey and Settlement at Tres Zapotes, in: C.A. Pool (Ed.), Settlement Archaeology and Political Economy at Tres Zapotes, Veracruz, Mexico, The Cotsen Institute of Archaeology, Monograph, vol. 50, University of California, Los Angeles, 2003, pp. 7–31.

[57] D.A. Hodell, M. Brenner, J.H. Curtis, T. Guilderson, Solar forcing of drought frequency in the Maya lowlands, Science 292 (2001) 1367–1370.

[58] T. Baumgartner, U. Struck, J. Alheit, GLOBEC investigation of interdecadal to multi-centennial variability in marine fish populations, Past Global Changes PAGES News, vol. 12 (1), 2004, pp. 19–21.

[59] J.A. Barron, D. Burky, J.L. Bischoff, A 2000-yr long record of climate from the Gulf of California, in: G.J. West, N.L. Blomquist (Eds.), Proceedings of the Nineteenth Pacific Climate Workshop, Asilomar, Pacific Grove, California, Technical Report 71 of the Interagency Ecological Program for the San Francisco Estuary, 2003, pp. 11–21.

[60] L. Vazquez-Selem, K. Heine, Late Quaternary glaciation of Mexico, in: J. Ehlers, P.L. Gibbard (Eds.), Quaternary Glaciations, Extent and Chronology, Part III, Elsevier, 2004, pp. 233–242.